nature chemistry

SUPPLEMENTARY INFORMATION

DOI: 10.1038/NCHEM.247

Amyloid β-Protein Oligomerization and the Importance of Tetramers and Dodecamers in the Aetiology of Alzheimer's Disease

Summer L. Bernstein, Nicholas F. Dupuis, Noel D. Lazo, Thomas Wyttenbach, Margaret M. Condron, Gal Bitan, David B. Teplow, Joan-Emma Shea, Brandon T. Ruotolo, Carol V. Robinson & Michael T. Bowers

Supplementary Discussion

The nano-ESI mass spectra for [Pro^{19}]Aβ40, [Met^{35}(O)]Aβ40 and [Met^{35}(O)]Aβ42 are shown in Supplementary Figure S1. Clearly all are similar, and similar to the WT spectrum for Aβ40 given in Figure 1 of the manuscript and Aβ42 given in reference 15 of the manuscript. All show a dominant z/n = -3 peak due to the direct transfer of this species from solution. In all cases this peak is almost exclusively monomer (n = 1). In contrast the z/n = -5/2 peaks are all composed of the -5 dimer and -10 tetramer with the exception of Aβ42 where higher-order oligomers are observed (see text).

The ATDs for the z/n = -5/2 peaks for all systems are given in Figure 2 of the text. Here we present the injection-energy dependence of the [Pro^{19}]Aβ40 and [Met^{35}(O)]Aβ40 ATDs for z/n = -2 in Supplementary Figure S2. Clearly the ATDs are composite and indicate significant amounts of monomer, dimer and trimer. This contrasts with the Aβ40 system where only monomers and dimers are observed (Figure 1, text). These results emphasize the fact that minor differences in primary structure can be amplified when the system aggregates.

The measured cross sections for all species discussed in the main text are given in Supplementary Tables S1 (Aβ40 alloforms) and S2 (Aβ42 alloforms). Reliable data for

all values of z/n for all alloforms could not be obtained either because that value of z/n was absent in the mass spectrum or it was too weak to measure. A plot of some of this data is given in Supplementary Figures S3a and b as σ/n versus n. The main points illustrated in these figures are that all values of σ/n decline with n due to accommodation as the system aggregates and that Aβ42 accommodates less as n increases than all other systems. These points are expanded on in the main text.

Model structures for Aβ alloform aggregates were obtained as follows. Each monomer was assumed to have a spherical shape. The three dimensionally averaged cross sections for the monomers were then obtained using the projection model (ref. 23, text) with the sphere radius as a variable parameter. This radius was adjusted to give the experimental monomer cross sections (Supplementary Tables S1 and S2). When these monomer "hard" spheres were used to calculate dimer and larger cross sections the model cross sections were much larger than experiment. This probably occurred due to multiple monomer structures contributing to the monomer cross section. Consequently it was decided to fit the dimer cross sections using the centre-centre distance (i.e. dimer diameter) of the two monomers as a variable parameter. This led to approximately a 10% overlap of the monomer spheres to reproduce the dimer experimental cross section. This degree of overlap was then maintained for all model structures calculated here. This process will produce model structures that are upper limits to more complex structures since the plots of σ/n vs. n continue to decrease as n increases. This indicates further accommodation occurs. Nonetheless this is not a large effect and the comparison of cross sections of model structures with experiment should allow global structures to be determined.

The strategy is to calculate extremes (largest possible structure and smallest possible structure) and reasonable candidates in between. For example, in Table 1 in the text, Aβ42 hexamer and dodecamer structures are calculated. The largest possible

hexamer (in the 3-D averaged sense) is linear and the smallest possible is the closest packed. The model cross sections from these limiting structures are obviously too large and too small respectively. A reasonable intermediate structure is the planar hexagon ring. As is apparent in the table good agreement with experiment is obtained. This doesn't prove this is the structure of this species but it is consistent with it and is the only reasonable symmetric structure that approximates experiment. Since the planar hexamer ring was found as the most probable hexamer structure, this was taken as the starting point of the dodecamer structure. The two limiting species that retained the hexamer ring are shown in Table 1 in the text. Clearly the stacked ring structure is in excellent agreement with experiment and the side-by-side structure is way too large.

A similar method was used for tetramer structures as shown in Figure 4 in the text. The limiting structures again are linear and closest packed. The closest packed structure was way too small in all cases so it is not included in the figure. The two intermediate structures shown are the planar hexagonal ring structure with one dimer removed and the planar square structure. The model cross sections of the structures are all divided by their respective linear cross sections so that all of them can fit on one normalized plot. This leads to a spread in the cross sections for the model intermediate structures shown by the arrows but doesn't interfere with the purpose of the figure. The dramatic result is that Aβ42 tetramer has a very different, more open structure than all other Aβ40 or Aβ42 alloforms. The apparent consequence of this structural difference is that Aβ42 goes on to form hexamer (paranuclei) and dodecamers while all other alloforms stop at the tetramer.

A second model was also developed. In this model the dimer cross sections were fit with smaller "touching but not overlapping" spheres. These spheres were then used to synthesize larger oligomer structures. The results are essentially the same as shown for the overlapping sphere model described above. A model similar to this has been

successfully used to obtain possible structures for assemblies of the larger trp RNA binding attenuation protein or TRAP (ref. 28, text).

The ATD for z/n = -5/2 of Aβ42 indicated that the dodecamer was the largest oligomer formed. We have identified the dodecamer structure as two stacked hexamers. The question is, why don't the hexamers keep stacking to form a 18mer, 24mer, etc. There are two plausible and possibly related reasons for this. First, the Aβ42 monomer is not a symmetric spherical species but a distribution of structures in solution (ref. 21 in text). Hence, the cyclic hexamer may well have distinct top and bottom sides. If so, there are three possible kinds of stacked hexamers: TB·BT, BT·TB, BT·BT (or TB·TB). Heterotypic stacking of the type BT·BT (or TB·TB) should produce a continuous distributions of oligomer order (refs. 24 and 25 in text) which is not observed here. Homotypic stacking (TB·BT or BT·TB) may occur because B·B or T·T interactions may be significantly stronger than other possibilities. This would lead to a terminal dodecamer oligomer as observed experimentally since further oligomerization should require binding of two weakly interacting surfaces.

A second, and possibly related reason for termination of oligomerization at the dodecamer is found in the structure of the hexamer itself. In a previous paper dealing with the structure of the Aβ42 monomer (ref. 21 in text) we speculated that the hexamer structure could well be composed of six monomers with their hydrophobic C-terminal tails pointed to the centre of the cyclic hexamer and the more hydrophilic N-terminal regions forming the outer surfaces of the cyclic species. The cartoon of the hexamer from reference 21 is reproduced in Supplementary Figure S4 (top left structure). When a dodecamer is formed these hydrophobic tails could well partially coalesce and the hydrophilic outer surfaces maximize their shielding potential. Schematically we show the structure in Figure S4. The resulting dodecamer would not add a third hexamer because it wouldn't participate in the hydrophobic stabilization as the dodecamer does.

Both of these mechanisms are plausible and it is likely a combination of them accounts for the termination of hexamer condensation in Aβ42 at the dodecamer.

In the ATDs presented here it is common for individual peaks to overlap. There can be two reasons for this. First, the two independent species have similar cross sections and the resolution of the instrument is not sufficient to separate them. In this case overlapped peaks occur even if a species has only one member in its family. The second reason that peaks can overlap is that each species has several stable family members with similar but slightly different cross sections. In this case each family has a broadened peak and overlap between families can occur even if there is sufficient resolution to resolve single member families. Here we will consider these issues for the ATDs of z/n = -5/2 of Aβ42 and Aβ40.

The z/n = -5/2 ATDs of Aβ42 and Aβ40 are given in Supplementary Figure S5 as the black lines. For the simple drift cell arrangement used in this work the ion transport equation can be solved analytically and is given in Supplementary Equation 1.

$$I(t) = \frac{I_o}{4(\pi D_L t)^{1/2}} \left(v_d + \frac{z}{t}\right) \left[1 - \exp\left(-\frac{r_o^2}{4D_T t}\right)\right] \exp\left[-\frac{(z - v_d t)^2}{4D_L t}\right] \quad (1)$$

This equation is valid for a packet of ions entering the cell through an orifice of radius r_0 at time t = 0. The ion packet drifts in a uniform electric field and undergoes both longitudinal diffusion (coefficient D_L) and transverse diffusion (coefficient D_T). After traversing the cell of length z at velocity v_d the ions exit the cell through a small on-axis orifice. To a good approximation both D_L and D_T can be obtained from the Einstein relationship

$$D = \frac{k_B T K}{e} \quad (2)$$

where e is the ion charge, T the temperature, K the (measured) ion mobility and k_B the Boltzmann constant. (Note: several small correction terms to Supplementary Equation 1 were utilized in obtaining the ATDs in Supplementary Figure S5 (see reference 32 in the text). Finally, the finite width of the injection pulse was accounted for by summing several distributions given by Supplementary Equation 1 with time shifted over the injection pulse width.

What is apparent in the figure is the dimer and tetramer experimental ATDs are broader than predicted for a species with a single mobility indicating there are several structures contributing to each with slightly different mobilities (cross sections). However, the experimental peak associated with the Aβ42 hexamer is essentially equivalent to the predicted peak shape as is the Aβ42 dodecamer. Hence, this is strong evidence there is only one hexamer structure and one dodecamer structure and structural self-selection occurs as the aggregation process proceeds. Given the data and arguments in the main text these are assigned as the planar symmetric cyclic structure for the hexamer and as two stacked hexamers for the dodecamer.

In order to attempt to observe higher-order aggregation in Aβ42, an experiment was done on a specially designed mass spectrometer (refs. 26 and 27 in the text). This instrument could be configured to maximize aggregation and detect it. The results are shown in Supplementary Figure S6. Clearly Aβ42 could be induced to form a broad, unresolved distribution of aggregates stretching from *m/z* 1000 to greater than 8000. An identical sample of [Pro^{19}]Aβ42, treated exactly the same, showed very little oligomerization, consistent with the fact [Pro^{19}]Aβ42 does not form fibrils.

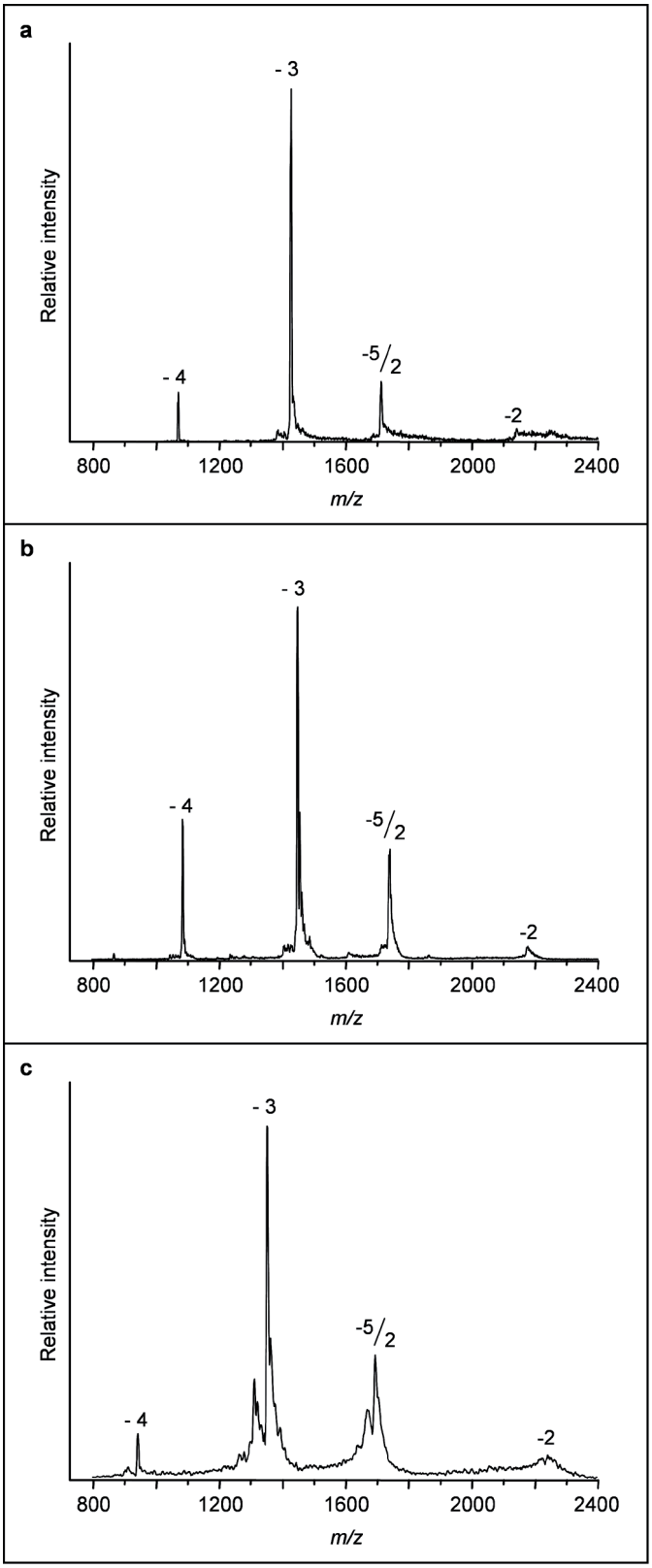

Supplementary Figure S1. Negative-ion mass spectra at 30 μM and pH 7.4 for (a) [Pro^{19}]Aβ40, (b) [Met^{35}(O)]Aβ40 and (c) [Met^{35}(O)]Aβ42. All peaks are labelled with their corresponding z/n value.

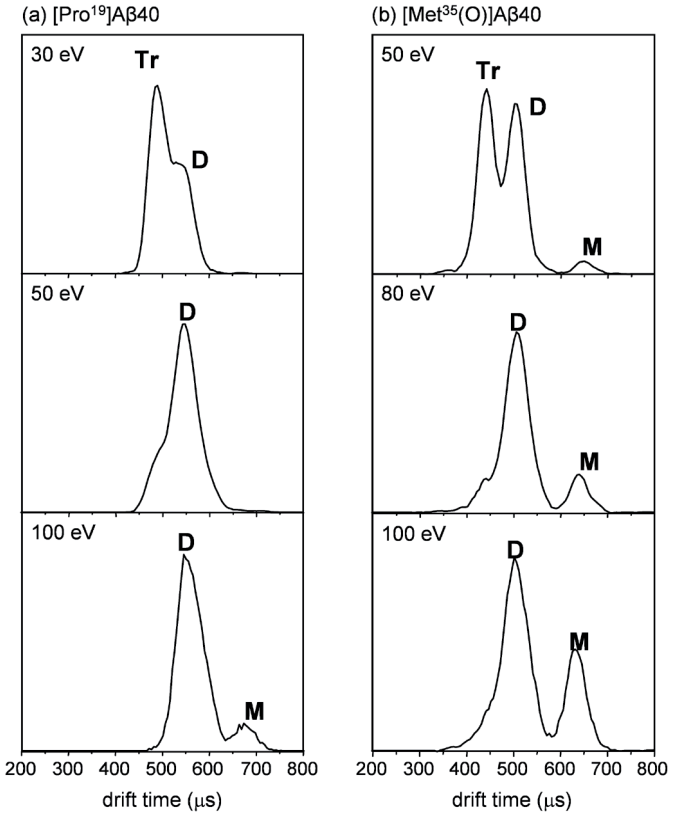

Supplementary Figure S2. (a) ATDs for [Pro^{19}]Aβ40 showing injection energy dependence for the -2 charge state at 30, 50 and 100 eV and for (b) [Met^{35}(O)]Aβ40 -2 charge state at 50, 80 and 100 eV. The peak designations are M = monomer, D = dimer and Tr = trimer.

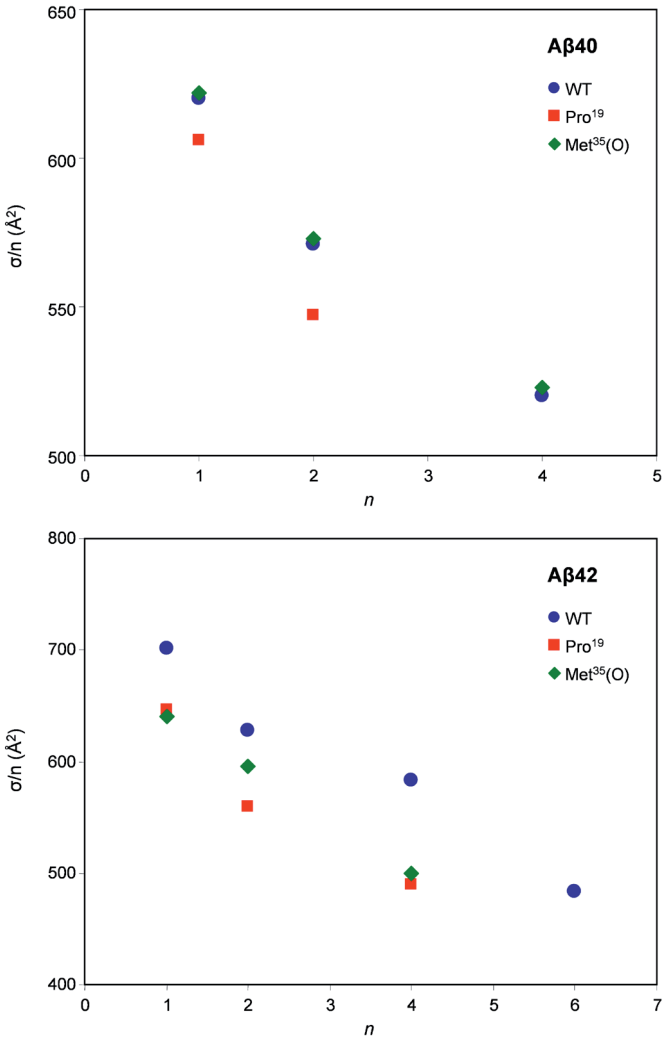

Supplementary Figure S3. Plot of σ/*n* in Å^2 versus *n*. For *n* = 1 the data are for *z*/*n* = -3 and for *n* > 1 for *z*/*n* = -5/2.

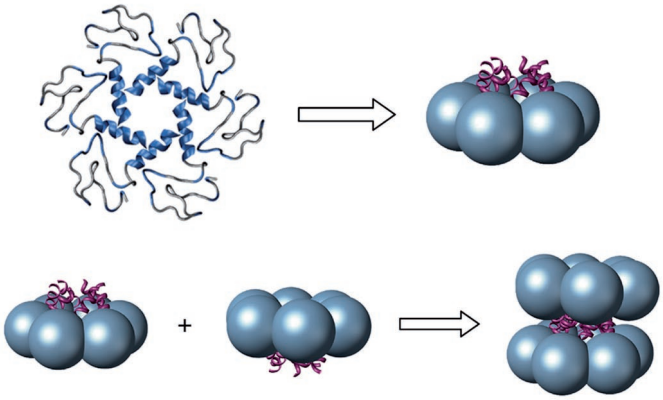

Supplementary Figure S4. Schematic mechanism for dihexamer formation. The cartoon at upper left is intended to emphasize that the hydrophobic tails of the six Aβ42 monomers are probably buried in the centre of the hexamer. In the spherical representation these hydrophobic tails are shown above and below the plane of the hexamer simply to indicate they are present. In the dodecamer the 12 hydrophobic tails are shown schematically shielded from the water solvent by the hydrophilic part of the peptides. This shielding could well be the reason a third hexamer can't add to the dodecamer explaining why the dodecamer is the terminal species observed in the experiment.

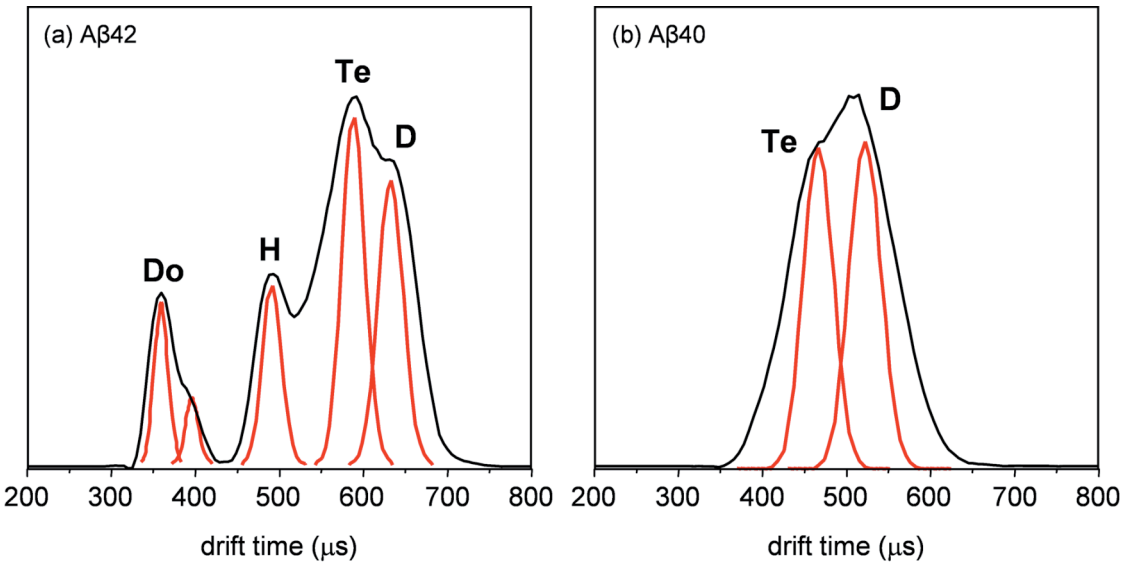

Supplementary Figure S5. Experimental *z/n* = -5/2 ATDs (black lines) with predicted distributions from Supplementary Equation 1 for each component shown in red for (a) Aβ42 and (b) Aβ40. D = dimer, Te = tetramer, H = hexamer and Do = dodecamer. Note the experimental dimer and tetramer portions of the ATDs are broader than the theoretical peaks for both Aβ40 and Aβ42 indicating several structures are present and contributing to the ATDs for these oligomers. However, the experimental ATDs for the hexamer and dodecamer (dihexamer) are much narrower and comparable to the theoretical line shapes indicating a single species for these structures.

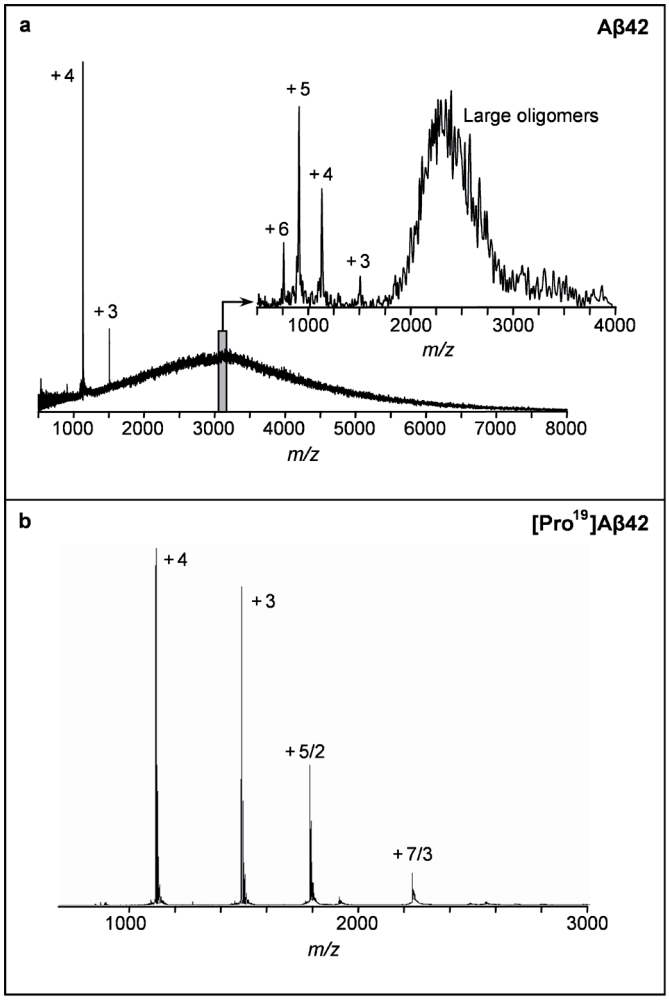

Supplementary Figure S6. Positive-ion mass spectra for Aβ42 alloforms taken on an instrument specially designed to observe oligomer states. (a) Aβ42 - inset is an MS/MS spectrum of a slice of the broad distribution near m/z = 3000. The broad feature near m/z = 2300 is unresolved oligomers and the narrow features labelled +3 to +6 are monomers. (b) [Pro^{19}]Aβ42 - spectrum taken under identical conditions as the spectrum in (a). Only small oligomers (at z/n = +5/2 and +7/3) are observed.

Supplementary Table S1. Cross Sections, σ (Å^2), for Aβ40 Alloforms

Oligomer	Charge State	Wild Type		Pro^{19}		Met^{35}(O)	
		σ	σ/*n* [a]	σ	σ/*n*	σ	σ/*n*
Monomer	-2	534	534	592	592	610	610
	-3	620	620	606	606	622	622
	-4	752	752	740	740	753	753
Dimer	-4	830	415	948	474	976	488
	-5	1142	571	1094	547	1145	573
Trimer	-6	–	–	1257	419	1275	425
Tetramer	-10	2080	520	–	–	2092	523

a) The value *n* = oligomer order

Supplementary Table S2. Cross Sections, σ (Å^2), for Aβ42 Alloforms

Oligomer	Charge State	Wild Type		Pro^{19}		Met^{35}(O)	
		σ	σ/*n* [a]	σ	σ/*n*	σ	σ/*n*
Monomer	-2	–	–	604	604	–	–
	-3	702	702	647	647	641	641
	-4	774	774	764	764	787	787
Dimer	-4	–	–	1060	530	–	–
	-5	1256	628	1120	560	1192	596
Trimer	-6	–	–	1446	482	–	–
Tetramer	-10	2332	583	1960	490	2000	500
Hexamer	-15	2898	483	–	–	–	–
Dipentamer	-25	3870	387	–	–	–	–
Dodecamer	-30	4308	359	–	–	–	–

a) The value *n* = oligomer order